

# Space–time Isogeometric Analysis of cardiac electrophysiology

Paola Francesca Antonietti<sup>1,3</sup>, Luca Dedè<sup>1</sup>, Gabriele Loli<sup>2</sup>, Monica Montardini<sup>2,3</sup>,  
Giancarlo Sangalli<sup>2,3</sup> and Paolo Tesini<sup>2,4,5</sup>

<sup>1</sup> MOX-Dipartimento di Matematica, Politecnico di Milano  
Piazza Leonardo da Vinci 32 - 20133, Milano, Italia  
{paola.antonietti, luca.dede}@polimi.it

<sup>2</sup> Dipartimento di Matematica “F. Casorati”, Università di Pavia  
Via A. Ferrata 5 - 27100, Pavia, Italia.  
{gabriele.loli, monica.montardini, giancarlo.sangalli, paolo.tesini}@unipv.it

<sup>3</sup> IMATI-CNR “Enrico Magenes”, Pavia, Italy.

<sup>4</sup> Dipartimento di Matematica e Applicazioni, Università degli Studi di Milano-Bicocca,  
Piazza dell’Ateneo Nuovo, 1 - 20126, Milano, Italia

<sup>5</sup> Dipartimento di Ingegneria Civile, Architettura, Territorio, Ambiente e di Matematica (DICATAM),  
Università degli Studi di Brescia, via Branze, 43 - 25123, Brescia, Italia

## Abstract

This work proposes a stable and efficient space-time method for the monodomain equation coupled with the Rogers–McCulloch ionic model, which is widely used to simulate electrophysiological wave propagation in the cardiac tissue. By extending the Spline Upwind method and exploiting low-rank matrix approximations, as well as preconditioned solvers, we achieve both significant computational efficiency and accuracy. In particular, we develop a formulation that is both simple and highly effective, designed to minimize spurious oscillations and ensuring computational efficiency. We rigorously validate the method’s performance through a series of numerical experiments, showing its robustness and reliability in diverse scenarios.

**Keywords:** Isogeometric Analysis, space–time, cardiac electrophysiology, Spline Upwind, efficient solvers

## 1 Introduction

Isogeometric Analysis (IgA), introduced in [1], is an advanced computational technique that extends the classical finite element method by using spline functions or their generalizations for both representing complex geometries and building the basis functions used in the approximation of partial differential equations. IgA enhances accuracy, especially in dealing with complex domains, due to its smooth spline properties, which offer higher accuracy compared to piecewise polynomials (see, e.g., [2, 3]) and compatibility with Computer Aided Design (CAD).

Space–time formulations in Isogeometric Analysis (IgA) present a valuable opportunity to leverage the properties of smooth splines in both space and time, as highlighted in references [4] and [5]. Notably, reference [5] focuses on the development of a stabilized IgA framework for the heat equation. In references [6] and [7], the authors introduce preconditioners and solvers to enhance computational efficiency. Furthermore, in [8] a continuous space–time IgA formulation to both linear and non-linear elastodynamics is applied.

This unified approach allows for a more seamless representation of the problem over time, but it also introduces challenges, particularly when sharp layers or fronts are present in the solution. These sharp layers can cause instabilities, such as spurious oscillations that propagate backward in time, leading to unphysical behaviors in the numerical solutions. To address this issue, the Spline Upwind method (SU) has been proposed in [9]. This method generalizes classical upwinding techniques, as SUPG [10], to stabilize space–time IgA formulations, ensuring more accurate and physically consistent results.

In the context of cardiac electrophysiology, the heart electrical activity is modeled by the bidomain or monodomain equations, which describe the propagation of electrical impulses across the heart tissue. These

models are crucial for understanding the heart function, particularly in simulating the action potential that triggers muscle contraction, with promising applications in diagnostic and predictive medicine and potentially supporting decision-making procedures in clinics (see, e.g., [11, 12]). The bidomain model divides the cardiac tissue into intracellular and extracellular spaces, governed by reaction–diffusion equations, while the monodomain model simplifies this assumption by setting equal anisotropic conductivities. References [11, 13] offer a comprehensive mathematical derivation of these equations.

An accurate representation of the ionic currents through ion channels is essential for realistic modeling of cardiac excitation. This requires coupling systems of ordinary differential equations with the monodomain equations. However, numerical challenges arise, particularly in resolving sharp fronts and traveling pulses, which are crucial for predicting heart activation.

Various strategies have been developed to address these issues, including modified quadrature rules [14], mesh adaptivity [15, 16, 17], and high-order spectral element discretizations [18]. These methods aim to achieve a balance between computational efficiency and solution accuracy.

To address these challenges, IgA has been effectively applied in cardiac electrophysiology, where the use of smooth functions enhances the accuracy of front speed simulations. In recent work [19], an innovative approach utilizing IgA on Non-Uniform Rational B-Spline (NURBS) surfaces has been proposed. The authors show that high-degree basis functions allow for precise front propagation with a reduced number of degrees of freedom. In a similar vein, always within the IgA framework, in [20] the Roger–McCulloch ionic model [21] is employed to address bidomain equations on surfaces. The results show that the use of B-splines effectively promotes the accuracy of the front propagation velocities and action potential shapes, yielding realistic simulations of atrial electrophysiology described with the Courtemanche–Ramirez–Nattel ionic model [22].

The aim of this work is to propose a stable and efficient space-time method for the monodomain equation coupled with the Rogers–McCulloch ionic model, by adapting the Spline Upwind method proposed in [9], originally developed for the heat equation, to make it computationally efficient for simulating electrophysiological wave propagation in cardiac tissue. Employing low-rank matrix approximation techniques and efficient preconditioned solvers enables us to tackle challenging problems that would otherwise demand excessive computational resources within the space-time framework.

In particular, preconditioners play a crucial role especially in the context of IgA space-time simulations on 3D spatial domains, where the complexity and size of the resulting linear systems can significantly impact on computational performance. Indeed, the application of preconditioners accelerates the iterative solver convergence of resulting linear system. For this reason, we propose suitable preconditioner, based on the previous construction of [7] and [23].

To evaluate the performance of the method, we present various numerical tests to investigate its numerical stability and computational cost.

The outline of the paper is as follows. The basics of IgA are presented in Section 2. In Section 3 we apply the stabilization method to the monodomain equation coupled with the Rogers–McCulloch ionic model. Numerical tests are analyzed in Section 4, while in Section 5 we draw conclusions.

## 2 Preliminary notions of IgA

We present the notation we use in subsequent sections.

Given  $n$  and  $p$  two positive integers, we consider the open knot vector

$$\widehat{\Xi} := \left\{ 0 = \widehat{\xi}_1 = \dots = \widehat{\xi}_{p+1} \leq \dots \leq \widehat{\xi}_n = \dots = \widehat{\xi}_{n+p+1} = 1 \right\},$$

and the vector  $\widehat{Z} := \{\widehat{\zeta}_1, \dots, \widehat{\zeta}_m\}$  of knots without repetitions, i.e., breakpoints.

The univariate spline space is defined as

$$\widehat{\mathcal{S}}_h^p := \text{span}\{\widehat{b}_{i,p}\}_{i=1}^n,$$

where  $\widehat{b}_{i,p}$  are the univariate B-splines and  $h$  is the mesh-size, i.e.,

$$h := \max\{|\widehat{\xi}_{i+1} - \widehat{\xi}_i| \text{ s.t. } i = 1, \dots, n+p\}.$$

To each univariate B-spline  $\widehat{b}_{i,p}$ , we associate a Greville abscissa, defined as

$$\gamma_{i,p} := \frac{\widehat{\xi}_{i+1} + \dots + \widehat{\xi}_{i+p}}{p} \quad \text{for } i = 1, \dots, n.$$

Multivariate B-splines are tensor product of univariate B-splines.

Just for the sake of simplicity, we consider splines of the same polynomial degree  $p_s \geq 1$  in all parametric spatial directions, while  $p_t \geq 1$  is the spline degree in time direction, and  $\mathbf{p} := (p_s, p_t)$ .

Given positive integers  $d$ ,  $n_l$ , for  $l = 1, \dots, d$  and  $n_t$ , we define  $d + 1$  univariate knot vectors  $\widehat{\Xi}_l := \{\widehat{\xi}_{l,1} \leq \dots \leq \widehat{\xi}_{l,n_l+p_s+1}\}$  for  $l = 1, \dots, d$  and  $\widehat{\Xi}_t := \{\widehat{\xi}_{t,1} \leq \dots \leq \widehat{\xi}_{t,n_t+p_t} + 1\}$  and  $d + 1$  breakpoints vectors  $\widehat{Z}_l := \{\widehat{\zeta}_{l,1}, \dots, \widehat{\zeta}_{l,m_l}\}$  for  $l = 1, \dots, d$  and  $\widehat{Z}_t := \{\widehat{\zeta}_{t,1}, \dots, \widehat{\zeta}_{t,m_t}\}$ . Moreover, let  $h_l$  be the mesh-size associated to  $\widehat{\Xi}_l$  for  $l = 1, \dots, d$ , and let  $h_t$  be the mesh-size associated to  $\widehat{\Xi}_t$ .

The multivariate B-splines are defined as

$$\widehat{B}_{\mathbf{i},\mathbf{p}}(\boldsymbol{\eta}, \tau) := \widehat{B}_{\mathbf{i}_s,p_s}(\boldsymbol{\eta}) \widehat{b}_{i_t,p_t}(\tau),$$

where

$$\widehat{B}_{\mathbf{i}_s,p_s}(\boldsymbol{\eta}) := \widehat{b}_{i_1,p_s}(\eta_1) \dots \widehat{b}_{i_d,p_s}(\eta_d),$$

$\mathbf{i}_s := (i_1, \dots, i_d)$ ,  $\mathbf{i} := (\mathbf{i}_s, i_t)$  and  $\boldsymbol{\eta} = (\eta_1, \dots, \eta_d)$ . The corresponding spline space is defined as

$$\widehat{\mathcal{S}}_h^{\mathbf{p}} := \text{span} \left\{ \widehat{B}_{\mathbf{i},\mathbf{p}} \mid i_l = 1, \dots, n_l \text{ for } l = 1, \dots, d; i_t = 1, \dots, n_t \right\},$$

where  $h := \max\{h_s, h_t\}$ . We have that  $\widehat{\mathcal{S}}_h^{\mathbf{p}} = \widehat{\mathcal{S}}_{h_s}^{p_s} \otimes \widehat{\mathcal{S}}_{h_t}^{p_t}$ , where

$$\widehat{\mathcal{S}}_{h_s}^{p_s} := \text{span} \left\{ \widehat{B}_{\mathbf{i}_s,p_s} \mid i_l = 1, \dots, n_l; l = 1, \dots, d \right\},$$

is the space of tensor-product splines on  $\widehat{\Omega} := (0, 1)^d$ , and

$$\widehat{\mathcal{S}}_{h_t}^{p_t} := \text{span} \left\{ \widehat{b}_{i_t,p_t} \mid i_t = 1, \dots, n_t \right\}.$$

Following [9], we assume that  $\widehat{\mathcal{S}}_{h_s}^{p_s} \subset C^0(\widehat{\Omega})$  and  $\widehat{\mathcal{S}}_{h_t}^{p_t} \subset C^{p_t-1}((0, 1))$ . The variable continuity in space may be useful for geometry representation. On the other hand, we consider only maximum continuity with respect to time in order to benefit from the approximation properties of smooth splines.

We denote by  $\Omega \times (0, T)$  the space-time computational domain, where  $\Omega \subset \mathbb{R}^d$  and  $\Omega$  is parametrized by  $\mathbf{F} : \widehat{\Omega} \rightarrow \Omega$ , with  $\mathbf{F} \in \left[ \widehat{\mathcal{S}}_{h_s}^{p_s} \right]^d$ , and  $T > 0$  is the final time. The space-time domain is parametrized by  $\mathbf{G} : \widehat{\Omega} \times (0, 1) \rightarrow \Omega \times (0, T)$ , such that  $\mathbf{G}(\boldsymbol{\eta}, \tau) := (\mathbf{F}(\boldsymbol{\eta}), T\tau) = (\mathbf{x}, t)$ .

The spline space with only initial condition, in parametric coordinates, is

$$\widehat{\mathcal{X}}_h := \left\{ \widehat{v}_h \in \widehat{\mathcal{S}}_h^{\mathbf{p}} \mid \widehat{v}_h = 0 \text{ on } \widehat{\Omega} \times \{0\} \right\}.$$

We also have that  $\widehat{\mathcal{X}}_h = \widehat{\mathcal{S}}_{h_s}^{p_s} \otimes \widehat{\mathcal{X}}_{t,h_t}$ , where

$$\widehat{\mathcal{X}}_{t,h_t} := \left\{ \widehat{w}_h \in \widehat{\mathcal{S}}_{h_t}^{p_t} \mid \widehat{w}_h(0) = 0 \right\} = \text{span} \left\{ \widehat{b}_{i_t,p_t} \mid i_t = 2, \dots, n_t \right\}.$$

With colexicographical re-orderings of the basis functions, we write

$$\widehat{\mathcal{X}}_h = \text{span} \left\{ \widehat{B}_{\mathbf{i},\mathbf{p}} \mid i = 1, \dots, N_{\text{dof}} \right\}, \quad (2.1)$$

$$\widehat{\mathcal{S}}_{h_s}^{p_s} := \text{span} \left\{ \widehat{B}_{\mathbf{i}_s,p_s} \mid i_s = 1, \dots, N_s \right\},$$

and

$$\widehat{\mathcal{S}}_{h_t}^{p_t} := \text{span} \left\{ \widehat{b}_{i_t,p_t} \mid i_t = 1, \dots, N_t \right\},$$

where  $N_{\text{dof}} := N_s N_t$ ,  $N_s := \prod_{l=1}^d n_l$ , with  $l = 1, \dots, d$  and  $N_t := n_t - 1$ .

Our isogeometric space is the isoparametric push-forward of (2.1) through the geometric map  $\mathbf{G}$ , i.e.,

$$\mathcal{X}_h := \text{span} \left\{ B_{\mathbf{i},\mathbf{p}} := \widehat{B}_{\mathbf{i},\mathbf{p}} \circ \mathbf{G}^{-1} \mid i = 1, \dots, N_{\text{dof}} \right\}, \quad (2.2)$$

where we can write  $\mathcal{X}_h = \mathcal{X}_{s,h_s} \otimes \mathcal{X}_{t,h_t}$ , with

$$\mathcal{X}_{s,h_s} := \text{span} \left\{ B_{i,p_s} := \widehat{B}_{i,p_s} \circ \mathbf{F}^{-1} \mid i = 1, \dots, N_s \right\},$$

and

$$\mathcal{X}_{t,h_t} := \text{span} \left\{ b_{i,p_t}(\cdot) := \widehat{b}_{i,p_t} \left( \frac{\cdot}{T} \right) \mid i = 1, \dots, N_t \right\}.$$

Finally, following [24], we define the support extension for  $\mathbf{i}_s := (i_1, \dots, i_d)$ , with  $i_l = 1, \dots, n_l$ ,  $l = 1, \dots, d$  and  $i_t = 1, \dots, N_t$ , as

$$\widetilde{I}_{\mathbf{i}_s, i_t} := \left( \widehat{\xi}_{1, i_1 - p_s}, \widehat{\xi}_{1, i_1 + p_s + 1} \right) \times \dots \times \left( \widehat{\xi}_{d, i_d - p_s}, \widehat{\xi}_{d, i_d + p_s + 1} \right) \times \left( \widehat{\xi}_{t, i_t - p_t}, \widehat{\xi}_{t, i_t + p_t + 1} \right).$$

To further explore the properties of B-splines and their application in IgA, we refer the reader to [25].

### 3 Spline Upwind for cardiac electrophysiology

In the context of cardiac electrophysiology, we consider the monodomain equation with the Rogers–McCulloch ionic model, proposed in [21]. The dimensionless unknowns are the transmembrane potential  $u$  and the recovery variable  $w$ , and the governing differential problem is

$$\begin{cases} C_m \partial_t u - D \Delta u + c_1 u(u - a)(u - 1) + c_2 u w = f & \text{in } \Omega \times (0, T), \\ \partial_t w - b(u - d_e w) = 0 & \text{in } \Omega \times (0, T), \\ \frac{\partial u}{\partial \mathbf{n}} = 0 & \text{on } \partial \Omega \times [0, T], \\ u = 0 & \text{in } \Omega \times \{0\}, \\ w = 0 & \text{in } \Omega \times \{0\}, \end{cases} \quad (3.1)$$

where  $\mathbf{n}$  is the exterior normal;  $a$ ,  $b$ ,  $c_1$ ,  $c_2$  and  $d_e$  are dimensionless positive parameters, specific of the Rogers–McCulloch model. The dimensionless constants  $C_m$  and  $D$  are the local membrane capacitance and the conductivity, respectively. In particular, the conductivity is very small with respect to the membrane capacitance. We assume that  $f \in L^2(\Omega \times (0, T))$ .

We consider the plain Galerkin method

find  $u_h, w_h \in \mathcal{X}_h$  such that

$$\begin{cases} \mathcal{A}(u_h, w_h; v_h) = \mathcal{F}(v_h) & \forall v_h \in \mathcal{X}_h, \\ \mathcal{L}(w_h, u_h; z_h) = 0 & \forall z_h \in \mathcal{X}_h, \end{cases} \quad (3.2)$$

where

$$\begin{aligned} \mathcal{A}(u_h, w_h; v_h) &:= \int_0^T \int_{\Omega} (C_m \partial_t u_h v_h + D \nabla u_h \cdot \nabla v_h + (c_1(u_h - a)(u_h - 1) + c_2 w_h) u_h v_h) \, d\Omega \, dt, \\ \mathcal{F}(v_h) &:= \int_0^T \int_{\Omega} f v_h \, d\Omega \, dt, \end{aligned} \quad (3.3)$$

and

$$\mathcal{L}(w_h, u_h; z_h) := \int_0^T \int_{\Omega} (\partial_t w_h z - b(u_h - d_e w_h) z_h) \, d\Omega \, dt.$$

We also consider the following stabilized formulation, based on Spline Upwind technique, introduced in [9]:

find  $u_h, w_h \in \mathcal{X}_h$  such that

$$\begin{cases} \mathcal{A}(u_h, w_h; v_h) + \mathcal{S}(u_h; v_h) = \mathcal{F}(v_h) & \forall v_h \in \mathcal{X}_h, \\ \mathcal{L}(w_h, u_h; z_h) = 0 & \forall z_h \in \mathcal{X}_h, \end{cases} \quad (3.4)$$

where for the stabilization terms  $\mathcal{S}(u_h; v_h)$ , we extend the definitions presented in [9]. In particular, the term  $\mathcal{S}(u_h; v_h)$  reads as follows

$$\mathcal{S}(u_h; v_h) := C_m \sum_{k=1}^p \int_0^T \tau_k(t) \int_{\Omega} \theta(\mathbf{x}, t) \partial_t^k u_h \partial_t^k v_h \, d\Omega \, dt,$$

where, for  $k = 1, \dots, p_t$ ,  $\tau_k(T \cdot) \in \widehat{\mathcal{S}}_{h_t}^{p_t-k} \subset C^{p_t-k-1}$  and are selected such that

$$\int_0^T b'_{\ell+i, p_t} b_{i, p_t} dt + \sum_{k=1}^{p_t} \int_0^T \tau_k(t) b_{\ell+i, p_t}^{(k)} b_{i, p_t}^{(k)} dt = 0,$$

for  $i = 1, \dots, N_t - 1$  and  $\ell = 1, \dots, r$ , with  $r = \min(p_t, N_t - i)$ , as in [9], and  $\theta(\mathbf{x}, t)$  denotes the function defined in the physical domain, which is associated with the  $(d+1)$ -linear interpolation of the following values computed in the parametric domain at the Greville abscissae, for  $i_l = 1, \dots, n_l$ ,  $l = 1, \dots, d$  and  $i_t = 1, \dots, N_t$ ,

$$\Theta_{i_s, i_t} := \min \left( \frac{\|C_m \partial_t u_h - D \Delta u_h + c_1 u_h (u_h - a)(u_h - 1) + c_2 u_h w_h - f\|_{L^\infty(\tilde{I}_{i_s, i_t})}}{C_m (T^{-1} \|u_h\|_{L^\infty(\Omega \times [0, T])} + \|\partial_t u_h\|_{L^\infty(\Omega \times [0, T])})}, 1 \right). \quad (3.5)$$

Finally, in order to speed up the computation of the stabilizing term, we consider a low-rank approximation of  $\theta$ . Given a relative tolerance  $\varepsilon > 0$ , using the algorithm in [26], we find  $R \in \mathbb{N}$  s.t.  $0 < R \leq \min(N_t, N_s)$ ,  $\mathbf{U} \in \mathbb{R}^{N_t \times R}$ ,  $\mathbf{V} \in \mathbb{R}^{N_s \times R}$  and  $\mathbf{R} \in \mathbb{R}^{R \times R}$  a diagonal matrix s.t.

$$\frac{\|\widehat{\Theta} - \mathbf{U} \mathbf{R} \mathbf{V}^T\|_{\mathbf{F}}}{\|\widehat{\Theta}\|_{\mathbf{F}}} \leq \varepsilon, \quad (3.6)$$

where  $\widehat{\Theta} \in \mathbb{R}^{N_t \times N_s}$  is obtained by reshaping the tensor (3.5) and  $\|\cdot\|_{\mathbf{F}}$  is the Frobenius norm.

In this way, we can write the function  $\theta(\mathbf{x}, t)$  as

$$\theta(\mathbf{x}, t) \approx \sum_{r=1}^R [\mathbf{R}]_{r,r} \theta_{t,r}(t) \theta_{s,r}(\mathbf{x}),$$

where  $\theta_{t,r}(t)$  is a linear interpolation of the  $r$ -th column of  $\mathbf{U}$ , on the Greville abscissae in the time direction and  $\theta_{s,r}(\mathbf{x})$  is a  $d$ -linear interpolation of  $r$ -th column of  $\mathbf{V}$ , on the Greville abscissae in the space directions.

Therefore, we have the following approximation

$$\mathcal{S}(u_h; v_h) \approx \widetilde{\mathcal{S}}(u_h; v_h) := C_m \sum_{r=1}^R [\mathbf{R}]_{r,r} \sum_{k=1}^p \int_0^T \tau_k(t) \theta_{t,r}(t) \int_{\Omega} \theta_{s,r}(\mathbf{x}) \partial_t^k u_h \partial_t^k v_h d\Omega dt. \quad (3.7)$$

### 3.1 Non-linear solver

We solve (3.2) and (3.4) by the following fixed point scheme:

given  $u_h^0, w_h^0 \in \mathcal{X}_h$ , the  $k+1$ -th iteration consists in finding  $\tilde{u}_h^{k+1}, \tilde{w}_h^{k+1} \in \mathcal{X}_h$  such that

$$\begin{cases} \mathcal{A}(\tilde{u}_h^{k+1}, u_h^k, w_h^k; v_h) + \widetilde{\mathcal{S}}(\tilde{u}_h^{k+1}; v_h) = \mathcal{F}(v_h) & \forall v_h \in \mathcal{X}_h, \\ \mathcal{L}(\tilde{w}_h^{k+1}; z_h) = \mathcal{G}(u_h^k; z_h) & \forall z_h \in \mathcal{X}_h, \end{cases} \quad (3.8)$$

where, with abuse of notation, in (3.8) we used

$$\mathcal{A}(\tilde{u}_h^{k+1}, u_h^k, w_h^k; v_h) := \int_0^T \int_{\Omega} (C_m \partial_t \tilde{u}_h^{k+1} v_h + D \nabla \tilde{u}_h^{k+1} \cdot \nabla v_h + C_r(u_h^k, w_h^k) \tilde{u}_h^{k+1} v_h) d\Omega dt,$$

with

$$C_r(u_h^k, w_h^k) := c_1 (u_h^k - a)(u_h^k - 1) + c_2 w_h^k, \quad (3.9)$$

$$\mathcal{L}(\tilde{w}_h^{k+1}; z_h) := \int_0^T \int_{\Omega} (\partial_t \tilde{w}_h^{k+1} z_h + b d_e \tilde{w}_h^{k+1} z_h) d\Omega dt \quad \text{and} \quad \mathcal{G}(u_h^k; z_h) := \int_0^T \int_{\Omega} b u_h^k z_h d\Omega dt,$$

while  $\mathcal{F}$  and  $\widetilde{\mathcal{S}}$  are defined in (3.3) and (3.7), respectively. System (3.8) consists of two decoupled equations, each of which can be solved independently.

Moreover, in order to promote the convergence of fixed point iterations, we introduce relaxation

$$u_h^{k+1} = \alpha \tilde{u}_h^{k+1} + (1 - \alpha) u_h^k \quad \text{and} \quad w_h^{k+1} = \alpha \tilde{w}_h^{k+1} + (1 - \alpha) w_h^k,$$

where we set  $\alpha = 0.5$ .

### 3.1.1 Discrete linear system

The linear systems resulting from (3.8) are

$$\mathbf{A}\tilde{\mathbf{u}}^{k+1} = \mathbf{f}, \quad (3.10)$$

$$\mathbf{L}\tilde{\mathbf{w}}^{k+1} = \mathbf{g}, \quad (3.11)$$

where  $[\mathbf{A}]_{i,j} := \mathcal{A}(B_{j,\mathbf{p}}, u_h^k, w_h^k; B_{i,\mathbf{p}})$ ,  $[\mathbf{L}]_{i,j} := (B_{j,\mathbf{p}}, B_{i,\mathbf{p}})$ ,  $[\mathbf{f}]_i := \mathcal{F}(B_{i,\mathbf{p}})$ ,  $[\mathbf{g}]_i := \mathcal{G}(B_{i,\mathbf{p}})$ . Exploiting the tensor-product structure of the isogeometric space  $\mathcal{X}_h$  (2.2), we have

$$\begin{aligned} \mathbf{A} &:= C_m \mathbf{W}_t \otimes \mathbf{M}_s + D \mathbf{M}_t \otimes \mathbf{K}_s + \mathbf{M}_R + C_m \sum_{r=1}^R [\mathbf{R}]_{r,r} \sum_{k=1}^p \mathbf{S}_{r,k}^t \otimes \mathbf{S}_{r,k}^s, \\ \mathbf{L} &:= (\mathbf{W}_t + b d_e \mathbf{M}_t) \otimes \mathbf{M}_s, \end{aligned}$$

where, using the definition (3.9), for  $i, j = 1, \dots, N_{\text{dof}}$  we have

$$[\mathbf{M}_R]_{i,j} = \int_0^T \int_{\Omega} C_r(u_h^k, w_h^k) B_{i,\mathbf{p}}(\mathbf{x}, t) B_{j,\mathbf{p}}(\mathbf{x}, t) \, d\Omega \, dt,$$

for  $i, j = 1, \dots, N_t$ ,

$$\begin{aligned} [\mathbf{S}_{r,k}^t]_{i,j} &= \int_0^T \tau_k(t) \theta_{t,r}(t) \partial_t^k b_{i,p_t}(t) \partial_t^k b_{j,p_t}(t) \, dt, \\ [\mathbf{W}_t]_{i,j} &= \int_0^T b'_{j,p_t}(t) b_{i,p_t}(t) \, dt \quad \text{and} \quad [\mathbf{M}_t]_{i,j} = \int_0^T b_{i,p_t}(t) b_{j,p_t}(t) \, dt, \end{aligned}$$

while, for  $i, j = 1, \dots, N_s$ ,

$$\begin{aligned} [\mathbf{S}_{r,k}^s]_{i,j} &= \int_{\Omega} \theta_{s,r}(\mathbf{x}) B_{i,p_s}(\mathbf{x}) B_{j,p_s}(\mathbf{x}) \, d\Omega, \\ [\mathbf{K}_s]_{i,j} &= \int_{\Omega} \nabla B_{i,p_s}(\mathbf{x}) \cdot \nabla B_{j,p_s}(\mathbf{x}) \quad \text{and} \quad [\mathbf{M}_s]_{i,j} = \int_{\Omega} B_{i,p_s}(\mathbf{x}) B_{j,p_s}(\mathbf{x}) \, d\Omega. \end{aligned}$$

## 3.2 Preconditioner

We consider for the linear system (3.10) the following preconditioner

$$[\widehat{\mathbf{A}}]_{i,j} = \widehat{\mathcal{A}}(\widehat{B}_{j,\mathbf{p}}, \widehat{B}_{i,\mathbf{p}})$$

where

$$\widehat{\mathcal{A}}(u, v) := \int_0^T \int_{\widehat{\Omega}} (C_m \partial_t u v + D \nabla u \cdot \nabla v + a c_1 u v) \, d\widehat{\Omega} \, dt.$$

We have that

$$\widehat{\mathbf{A}} = C_m \mathbf{W}_t \otimes \widehat{\mathbf{M}}_s + \mathbf{M}_t \otimes (D \widehat{\mathbf{K}}_s + a c_1 \widehat{\mathbf{M}}_s), \quad (3.12)$$

where for  $i, j = 1, \dots, N_s$

$$[\widehat{\mathbf{K}}_s]_{i,j} = \int_{\widehat{\Omega}} \nabla \widehat{B}_{i,p_s}(\mathbf{x}) \cdot \nabla \widehat{B}_{j,p_s}(\mathbf{x}) \quad \text{and} \quad [\widehat{\mathbf{M}}_s]_{i,j} = \int_{\widehat{\Omega}} \widehat{B}_{i,p_s}(\mathbf{x}) \widehat{B}_{j,p_s}(\mathbf{x}) \, d\widehat{\Omega}$$

are the stiffness and mass matrices in the parametric domain, respectively. It also holds

$$\widehat{\mathbf{K}}_s = \sum_{i=1}^d \widehat{M}_d \otimes \dots \otimes \widehat{M}_{i+1} \otimes \widehat{K}_i \otimes \widehat{M}_i \otimes \dots \otimes \widehat{M}_1 \quad \text{and} \quad \widehat{\mathbf{M}}_s = \widehat{M}_d \otimes \dots \otimes \widehat{M}_1,$$

where  $\widehat{K}_l$  and  $\widehat{M}_l$  are the univariate stiffness and mass matrices, respectively. To apply the preconditioner (3.12), we generalize the technique proposed in [7]. Thus, following [7], we consider the generalized eigendecomposition of the pencils  $(\widehat{\mathbf{K}}_l, \widehat{\mathbf{M}}_l)$  for  $l = 1, \dots, d$ , which gives the matrices  $\mathbf{U}_l$  for  $l = 1, \dots, d$  for  $l = 1, \dots, d$ , that contain

in each column the  $\widehat{\mathbf{M}}_l$ -orthonormal generalized eigenvectors and  $\mathbf{\Lambda}_l$  that are diagonal matrices whose entries contain the corresponding generalized eigenvalues. Moreover, we define

$$[\mathbf{w}]_i = [\mathbf{W}_t]_{i,N_t} \quad \text{and} \quad [\mathbf{m}]_i = [\mathbf{M}_t]_{i,N_t} \quad \text{for} \quad i = 1, \dots, N_t - 1,$$

$$[\overset{\circ}{\mathbf{W}}_t]_{i,j} = [\mathbf{W}_t]_{i,j} \quad \text{and} \quad [\overset{\circ}{\mathbf{M}}_t]_{i,j} = [\mathbf{M}_t]_{i,j} \quad \text{for} \quad i, j = 1, \dots, N_t - 1.$$

and we consider the matrices  $\overset{\circ}{\mathbf{U}}_t$  and  $\mathbf{\Lambda}_t$ , that are the matrix whose columns contain the  $\overset{\circ}{\mathbf{M}}_t$ -orthogonal generalized eigenvectors of the pencil  $(\overset{\circ}{\mathbf{W}}_t, \overset{\circ}{\mathbf{M}}_t)$  and the matrix of the corresponding eigenvalues, respectively. We then define the matrix  $\mathbf{U}_t$  as

$$\mathbf{U}_t := \begin{bmatrix} \overset{\circ}{\mathbf{U}}_t & \mathbf{t} \\ \mathbf{0}^T & \rho \end{bmatrix},$$

where  $\mathbf{0} \in \mathbb{R}^{N_t-1}$  denotes the null vector, while

$$\begin{bmatrix} \mathbf{t} \\ \rho \end{bmatrix} := \frac{\begin{bmatrix} \mathbf{v} \\ 1 \end{bmatrix}}{\left( [\mathbf{v}^* \ 1] \mathbf{M}_t \begin{bmatrix} \mathbf{v} \\ 1 \end{bmatrix} \right)^{\frac{1}{2}}},$$

and  $\mathbf{v} \in \mathbb{C}^{N_t-1}$  such that

$$\overset{\circ}{\mathbf{M}}_t \mathbf{v} = -\mathbf{m}.$$

Finally, we set  $\mathbf{\Delta}_t := \mathbf{U}_t^* \mathbf{W}_t \mathbf{U}_t$ . The matrix  $\mathbf{\Delta}_t$  has an arrowhead structure (see [7] for details).

Then, factorizing the common terms, we get that  $\widehat{\mathbf{A}}$  can be written as

$$\widehat{\mathbf{A}} = (\mathbf{U}_t^* \otimes \mathbf{U}_s^T)^{-1} (C_m \mathbf{\Delta}_t \otimes \mathbb{I}_{N_s} + D \mathbb{I}_{N_t} \otimes \mathbf{\Lambda}_s + a c_1 \mathbb{I}_{N_t} \otimes \mathbb{I}_{N_s}) (\mathbf{U}_t \otimes \mathbf{U}_s)^{-1}, \quad (3.13)$$

where  $\mathbf{\Lambda}_s := \sum_{l=1}^d \mathbb{I}_{n_d} \otimes \dots \otimes \mathbb{I}_{n_{l+1}} \otimes \mathbf{\Lambda}_l \otimes \mathbb{I}_{n_{l-1}} \otimes \dots \otimes \mathbb{I}_{n_1}$ ,  $\mathbf{U}_s := \mathbf{U}_d \otimes \dots \otimes \mathbf{U}_1$  and  $\mathbb{I}_n$  denotes the identity of dimension  $n \times n$ . Note that the second term of (3.13) exhibits a block-arrowhead structure:

$$C_m \mathbf{\Delta}_t \otimes \mathbb{I}_{N_s} + D \mathbb{I}_{N_t} \otimes \mathbf{\Lambda}_s + a c_1 \mathbb{I}_{N_t} \otimes \mathbb{I}_{N_s} = \begin{bmatrix} \mathbf{H}_1 & & & \mathbf{B}_1 \\ & \ddots & & \vdots \\ & & \mathbf{H}_{N_t-1} & \mathbf{B}_{N_t-1} \\ -\mathbf{B}_1^* & \dots & -\mathbf{B}_{N_t-1}^* & \mathbf{H}_{N_t} \end{bmatrix},$$

where  $\mathbf{H}_i$  and  $\mathbf{B}_i$  are diagonal matrices defined as

$$\mathbf{H}_i := C_m [\mathbf{\Lambda}_t]_{i,i} \mathbb{I}_{N_s} + D \mathbf{\Lambda}_s + a c_1 \mathbb{I}_{N_s} \quad \text{and} \quad \mathbf{B}_i := C_m [\mathbf{g}]_i \mathbb{I}_{N_s} \quad \text{for} \quad i = 1, \dots, N_t - 1,$$

$$\mathbf{H}_{N_t} := C_m \sigma \mathbb{I}_{N_s} + D \mathbf{\Lambda}_s + a c_1 \mathbb{I}_{N_s},$$

while  $\mathbf{g} := \overset{\circ}{\mathbf{U}}_t^* \begin{bmatrix} \overset{\circ}{\mathbf{W}}_t & \mathbf{w} \\ \rho \end{bmatrix}$  and  $\sigma := [\mathbf{t}^* \rho^*] \mathbf{W}_t \begin{bmatrix} \mathbf{t} \\ \rho \end{bmatrix}$ . This property is used in the application of the preconditioner (3.13), that we perform with [7, Algorithm 1 Extended FD]. Parallelization presents a further opportunity for enhancing computational efficiency, but is not adopted in this paper.

We now focus on the solution of (3.11): we note that, exploiting the properties of the Kronecker product, the solution can be obtained as

$$\mathbf{w} = \text{vec} \left( \mathbf{M}_s^{-1} \mathbf{G} (\mathbf{W}_t + b d_e \mathbf{M}_t)^{-\top} \right),$$

where the “vec” operator applied to a matrix stacks its columns into a vector, and  $\mathbf{G}$  is the  $N_s \times N_t$  matrix such that  $\mathbf{g} = \text{vec}(\mathbf{G})$ . Therefore,  $\mathbf{w}$  can be computed by solving  $N_s$  independent systems associated with the  $N_t \times N_t$  matrix  $(\mathbf{W}_t + b d_e \mathbf{M}_t)^\top$ , as well as  $N_t$  independent systems associated with the  $N_s \times N_s$  spatial mass matrix  $\mathbf{M}_s$ . For the latter we can efficiently leverage the preconditioner proposed in [23].

## 4 Numerical Results

All numerical tests are performed using MATLAB with GeoPDEs [27] and Tensorlab [28] on Intel(R) Xeon(R) Gold 6130 CPU processor, running at 2.10 GHz and with 128 GB of RAM. We use B-splines with the maximum continuity allowed and uniform meshes along each parametric direction and we consider the same polynomial degree for space and time, i.e.,  $p_s = p_t =: p$ .

Following [21], we set  $a = 0.13$ ,  $b = 0.013$ ,  $c_1 = 0.26$ ,  $c_2 = 0.1$  and  $d_e = 1$ .

For the low-rank approximation (3.6), we use `svdsketch` MATLAB function with  $\varepsilon = 10^{-1}$  and the fixed point method, presented in Section 3.1, is used to solve nonlinearities in the equations, with the stopping criterion:  $\|u_h^{k+1} - u_h^k\|_\infty \leq \delta$ , with  $\delta = 10^{-4}$ .

In the numerical experiments,  $\chi_{[\bar{\psi}_1, \bar{\psi}_2]}(\psi)$  refers to the characteristic function, defined as

$$\chi_{[\bar{\psi}_1, \bar{\psi}_2]}(\psi) := \begin{cases} 1 & \text{for } \psi \in [\bar{\psi}_1, \bar{\psi}_2], \\ 0 & \text{otherwise.} \end{cases}$$

### 4.1 Test with smooth solution

We deal with a smooth solution on all the space-time domain  $\Omega \times (0, 1)$ , with  $\Omega = (0, 1)$ , to analyze the convergence order of SU method. We set  $C_m = 1$  and  $D = 10^{-4}$ .

Moreover, in this test, we neglect the action of the recovery variable, i.e., we fix a null value for  $w$  and we do not introduce the relaxations presented in Section 3.1.

We compute the function  $f$  in (3.1) in order to generate an exact solution  $u_{\text{ex}} = 10 \sin(\pi x) \sin(\pi t) (1 - \exp(-x))(1 - \exp(x - 1))(1 - \exp(t - 1))$ . The resulting linear systems are solved by direct solver provided by MATLAB (backslash operator "\").

Figure 1 shows the error plot in  $L^2$ -norm for SU method with uniform meshes in space and time, i.e.,  $h_1 = h_t =: h$  and B-spline degrees  $p = 2, 3$ , exhibiting optimal convergence order.

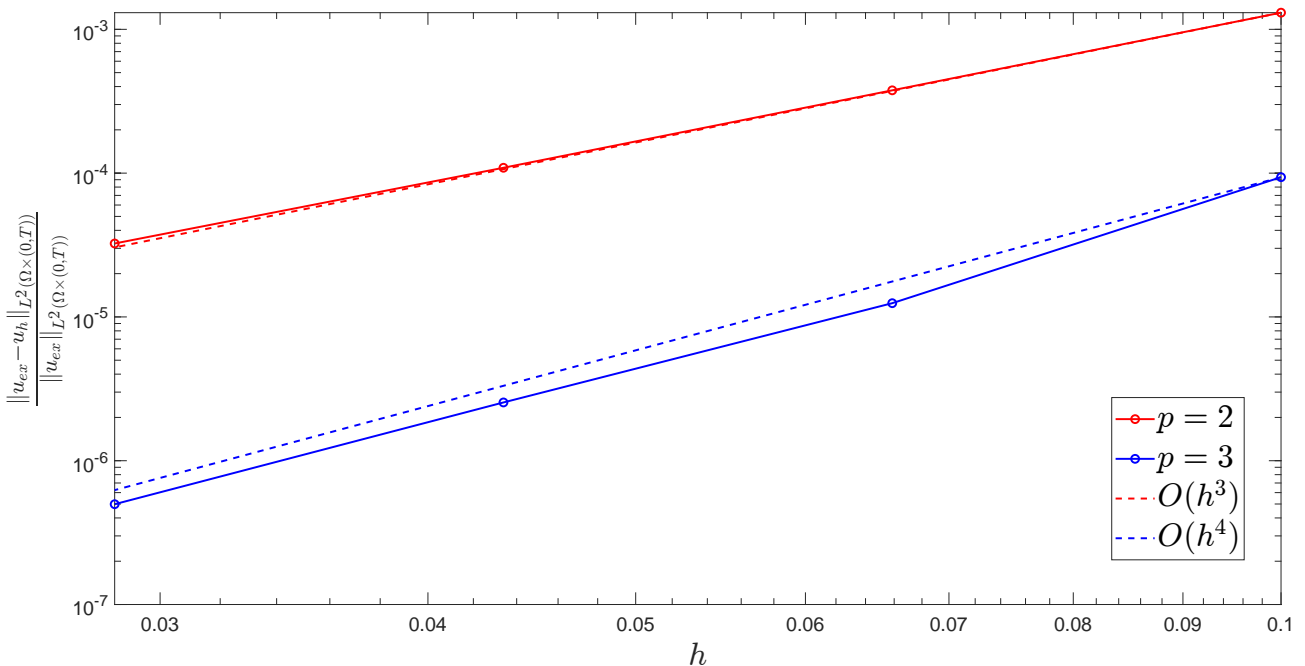


Figure 1: SU relative error plots in  $L^2$ -norm.

### 4.2 2D spatial domain

In this Section we consider an ellipse (semi-major axis:  $a_o = 0.75$ ; semi-minor axis:  $b_o = 0.125$ ) with an elliptic hole (semi-major axis:  $a_i = 0.375$ ; semi-minor axis:  $b_i = 0.0625$ ) as spatial domain  $\Omega$  (Figure 2), while  $(0, T)$ , with  $T = 300$ , is time domain. We set  $C_m = 1$  and  $D = 10^{-4}$ .



We consider  $h_1 = 2^{-6}$ ,  $h_2 = 2^{-3}$ ,  $h_t = 2^{-5}$  and  $p = 3$ . The resulting linear systems are solved by direct solver provided by MATLAB (backslash operator "\").

The source term  $f$  is as follows:

$$f(x, y, t) = 1/4 \exp\left(-\left(5 \cdot 10^2 \left((y - L_2/2)^2 + (x - 8/15 L_1/T t)^2\right)\right)\right) \chi_{[90,100]}(t),$$

where  $L_2 = 0.125$  and  $L_1 = 1.5$ .

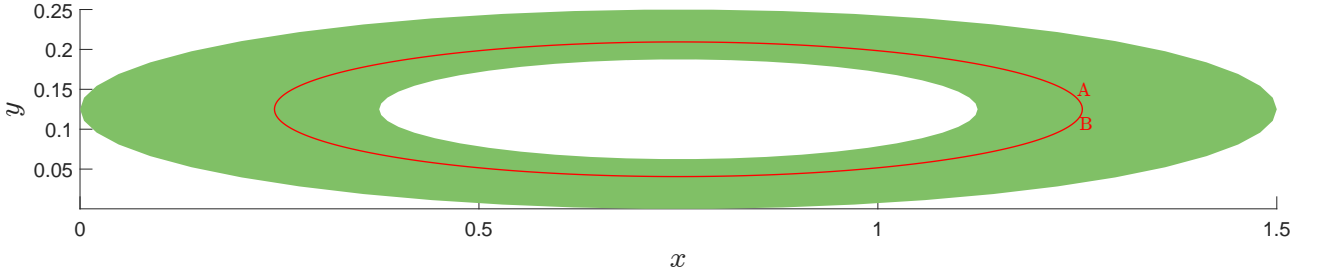


Figure 2: 2D spatial domain with section line  $s$  (A–B), test in Section 4.2.

Figures 3 and 4 show the numerical solutions along section line  $s$  (depicted in Figure 2) of the plain Galerkin and SU methods, while the function  $\theta(x, y, t)$ , regulating the Spline Upwind activation, is presented in Figure 5. Furthermore, Figure 6 shows the SU method solutions for various fixed times. In this test the plain Galerkin method presents spurious oscillation and these numerical instabilities are negligible in SU method.

Table 1 shows that the computational time of the plain Galerkin method is considerably higher compared to that of the SU method. This result is due to the high number of iterations required to reach the set convergence, caused by considerable numerical instabilities.

	Fixed point iterations	Time (s)
Standard Galerkin method	145	$1.0 \cdot 10^4$
SU method	31	$2.7 \cdot 10^3$

Table 1: Computational cost comparison for 2D spatial domain, test in Section 4.2.

### 4.3 3D spatial domain

For this test we use the 3D spatial domain  $\Omega$  shown in Figure 7, which approximates the structure of the left ventricle, and  $(0, T)$ , with  $T = 300$ , is time domain, while  $p = 2$ . We set  $C_m = 1$  and  $D = 10^{-3}$ , to simulate the propagation of the impulse under physiological conditions, while we consider  $h_1 = h_2 = h_3 = 2^{-4}$  and  $h_t = 2^{-6}$ .

The linear systems (3.10) are solved using the generalized minimal residual method (GMRES) preconditioned as presented in Section 3.2. Concerning (3.11), we exploit the technique presented Section 3.2 and we solve  $N_s$  independent systems associated with the  $N_t \times N_t$  matrix with direct solver provided by MATLAB (backslash operator "\"), while  $N_t$  independent systems associated with the  $N_s \times N_s$  mass matrix are solved by using the preconditioned conjugate gradient method (PCG). We fix the tolerance for both methods equal to  $10^{-8}$  and we use the preconditioner described in Section 3.2.

The source term  $f$  is as follows:

$$f(\eta_1, \eta_2, \eta_3, t) = 1/10 \chi_{[0.9,1]}(\eta_3) \chi_{[45,60]}(t).$$

Figures 8 and 9 compare the numerical solutions obtained with the plain Galerkin method and the SU method at various fixed times. Before the activation of the source term (i.e., for  $t < 45$ ), where zero transmembrane potential is expected, Figure 8 shows non-physical behaviors in the plain Galerkin solutions, indicating numerical instabilities. On the other hand, Figure 9 suggests that the SU method effectively suppresses these oscillations: before the activations of the source term, the solutions correctly remain zero in the spatial domain.

Table 2 presents the total computational time to solve the problem numerically and the average number of GMRES e PCG solvers iterations for each fixed-point iteration. In particular, the SU method requires one and a half times the total computation time of the plain Galerkin method.

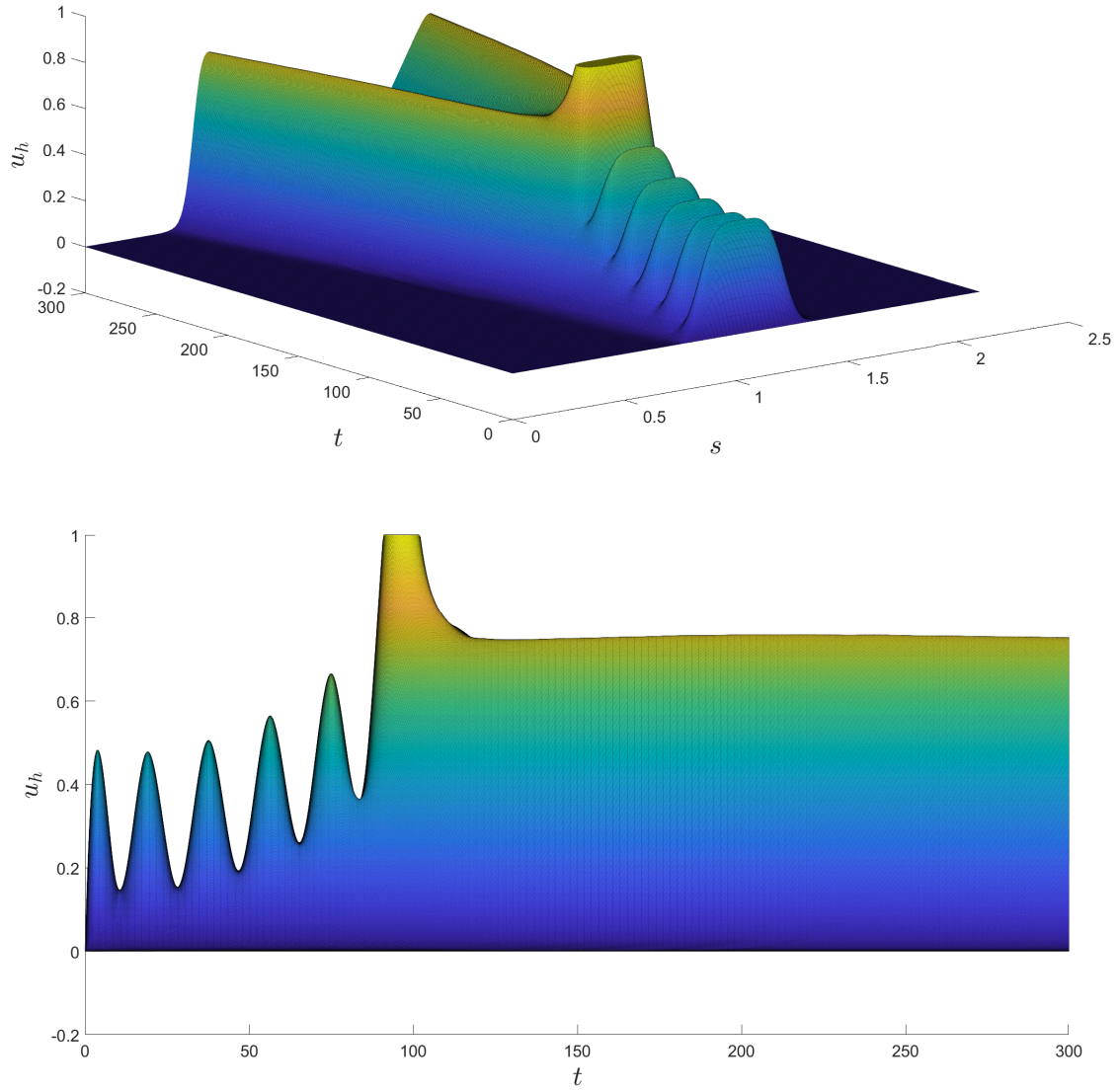


Figure 3: Two views of plain Galerkin transmembrane potential  $u_h$  along section line  $s$  on 2D spatial domain, test in Section 4.2.

	GMRES, PCG average iterations	Fixed-point iterations	Time (s)
Standard Galerkin method	115, 4	41	$8.7 \cdot 10^3$
SU method	132, 4	39	$1.3 \cdot 10^4$

Table 2: Computational cost comparison for 3D spatial domain, test in Section 4.3.

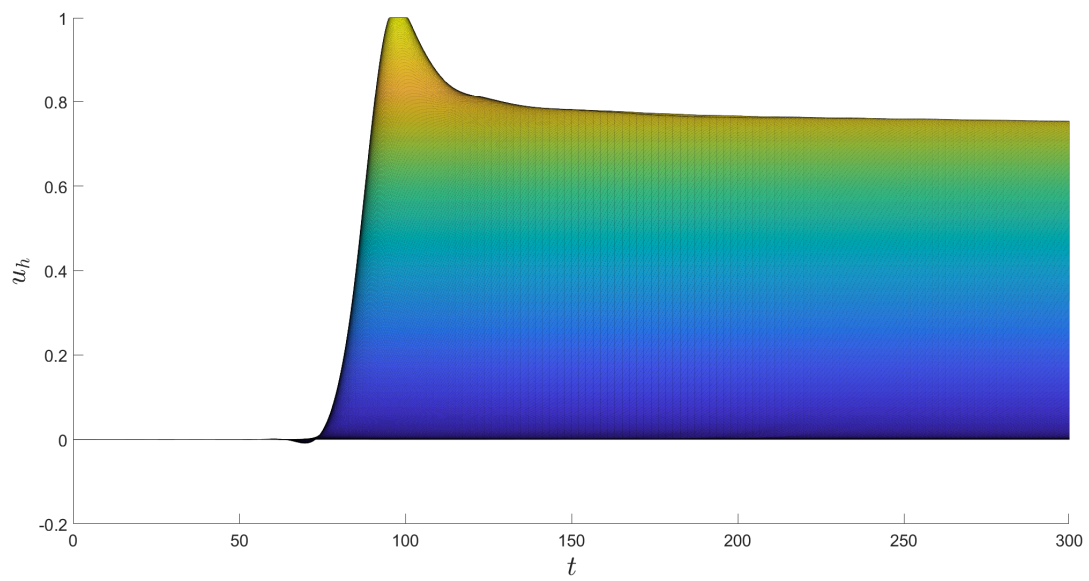
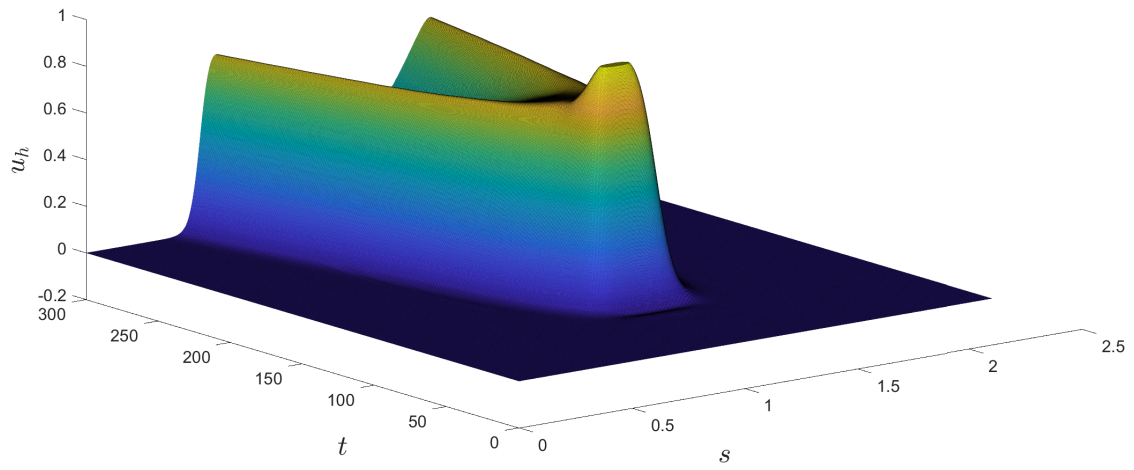


Figure 4: Two views of SU transmembrane potential  $u_h$  along section line  $s$  on 2D spatial domain, test in Section 4.2.

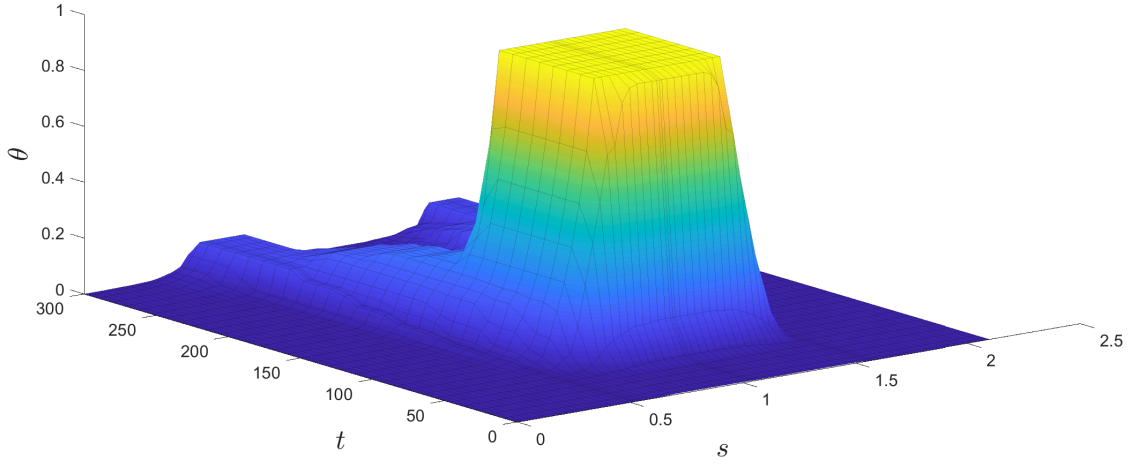


Figure 5: The function  $\theta(x, y, t)$  along section line  $s$  on 2D spatial domain, test in Section 4.2.

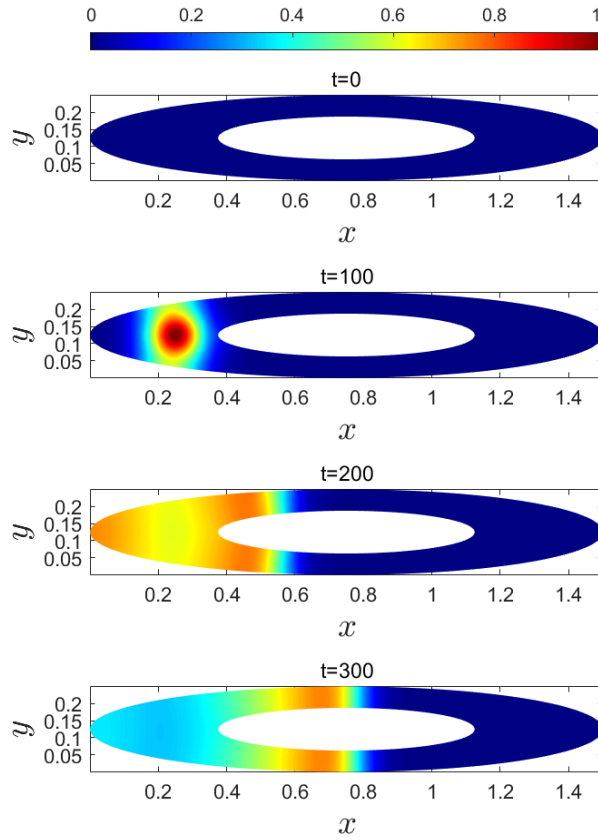


Figure 6: SU transmembrane potential, for various fixed times on 2D spatial domain, test in Section 4.2.

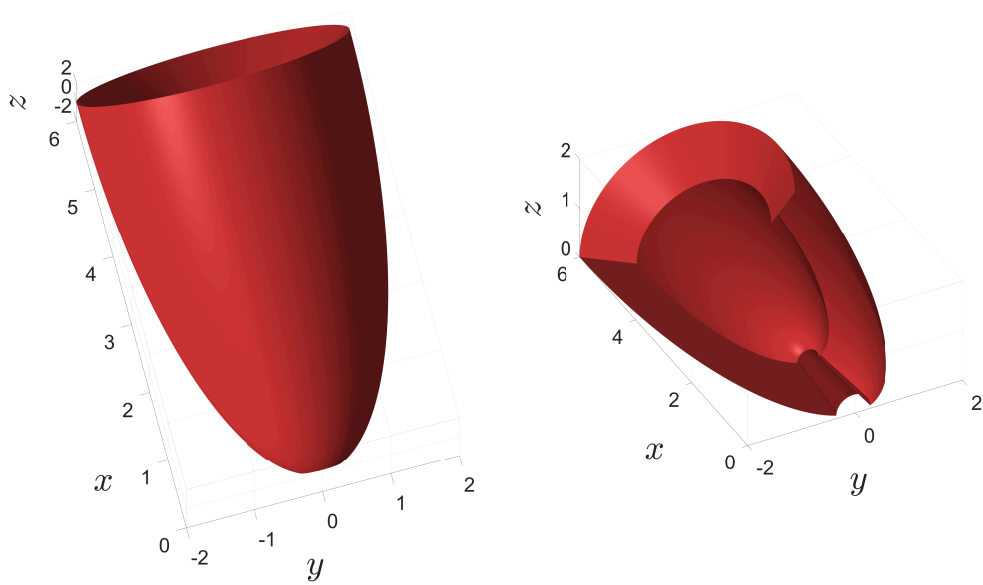


Figure 7: Ventricular spatial domain  $\Omega$  for the test in Section 4.3 on the left, and its corresponding cross-section for solution plots on the right.

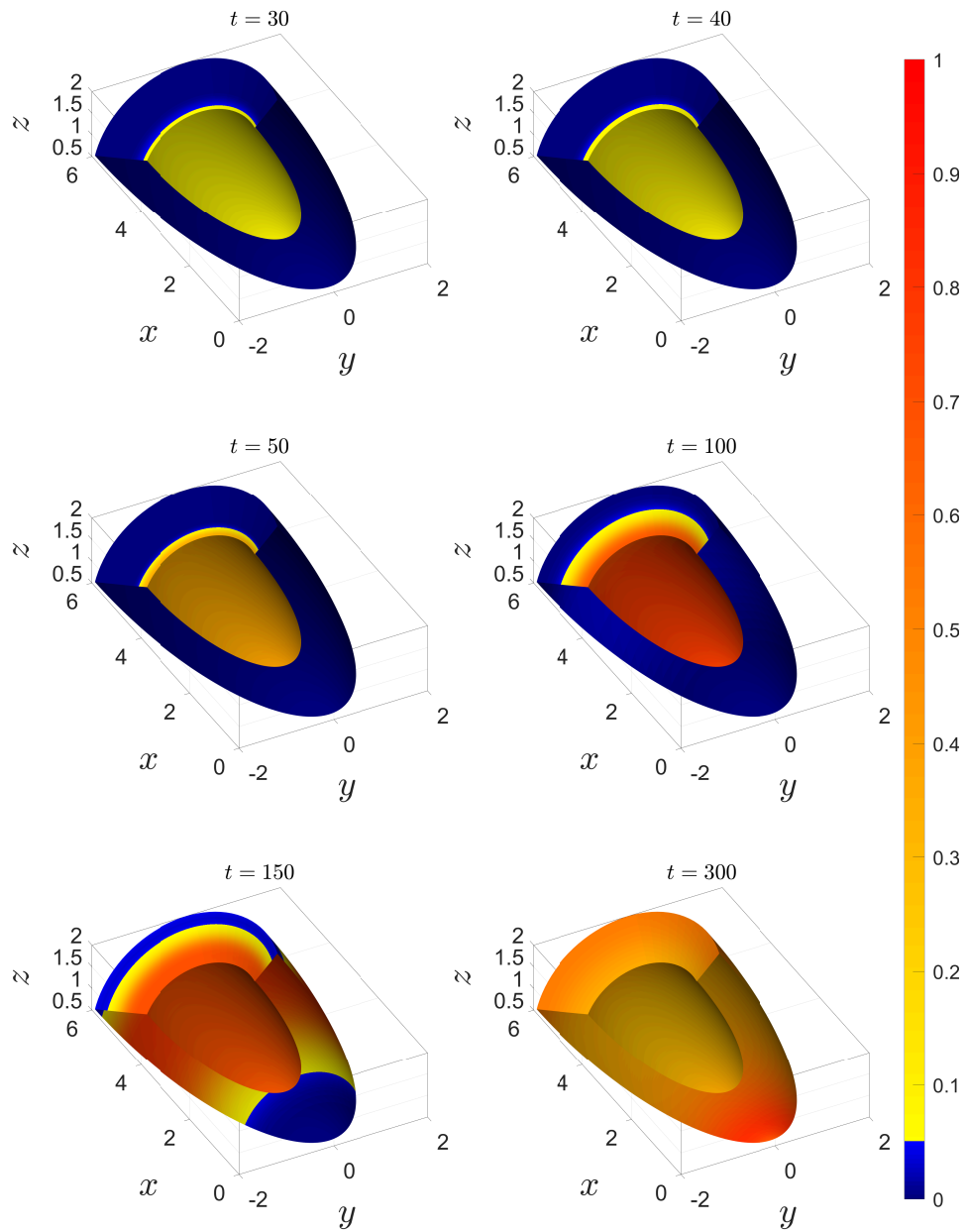


Figure 8: Plain Galerkin transmembrane potential, for various fixed times on 3D spatial domain, test in Section 4.3.

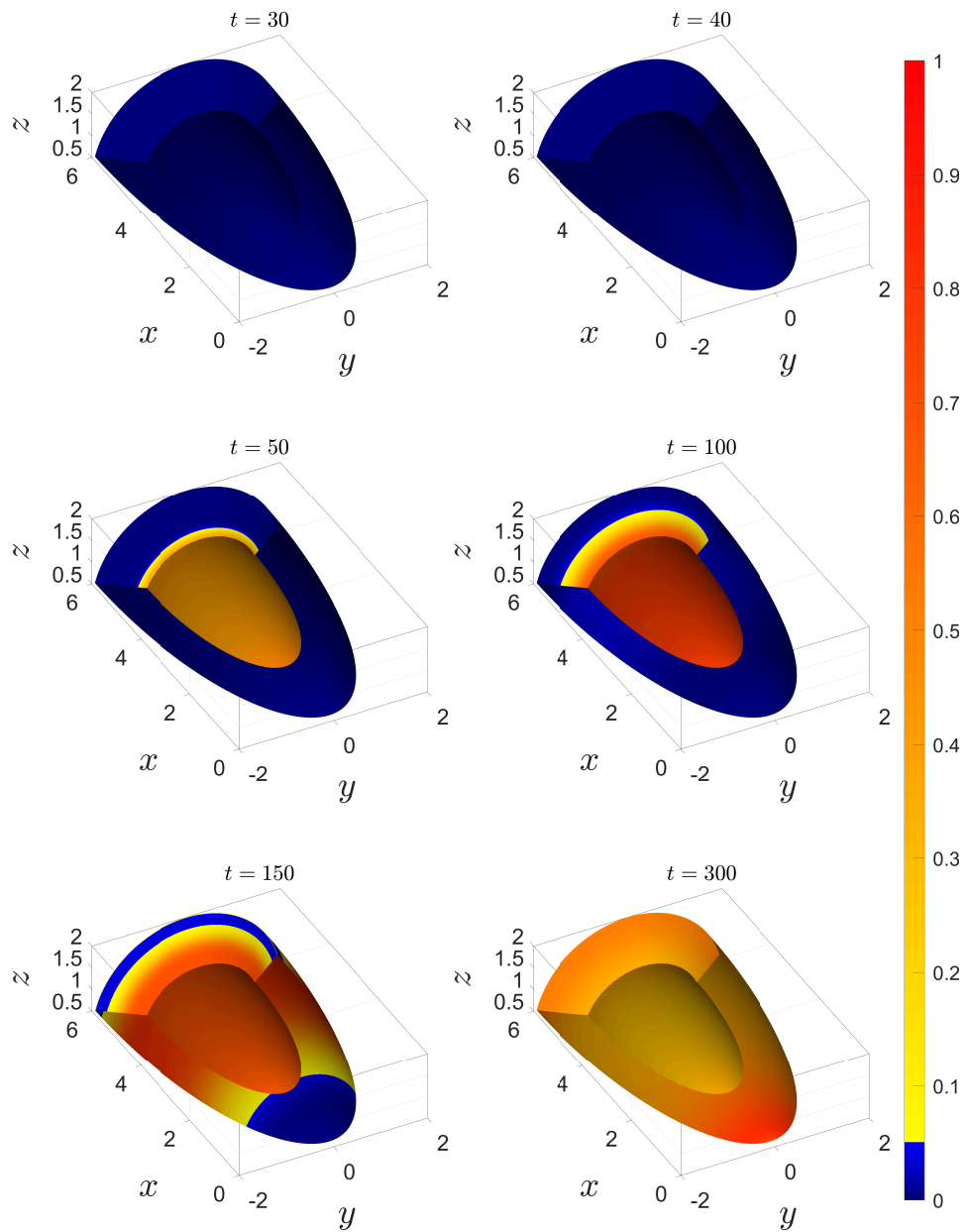


Figure 9: SU transmembrane potential, for various fixed times on 3D spatial domain, test in Section 4.3.

## 5 Conclusions

We proposed a solver to prevent spurious oscillations for evolutionary problems related to cardiac electrophysiology in the space–time IgA framework. We used a variant of the Spline Upwind (SU) method introduced in [9].

The numerical tests highlight the optimal convergence order for smooth solution and the stable behavior in the presence of sharp layers in the monodomain equation with the Rogers–McCulloch ionic model, both in two-dimensional and three-dimensional spatial domains.

To complete the analysis, we quantified the computational cost in terms of the number of iterations required by the nonlinear solvers to obtain the solution, as well as the corresponding time. In our tests, transitioning from the plain Galerkin method to the SU method, we have showed that the computational times of the SU method are competitive with those of the plain Galerkin method. This makes SU stabilization appealing not only in terms of solution stability but also in terms of computational efficiency.

Finally, we emphasize the importance of efficient and fast solvers in the space–time framework: the higher dimensionality poses computational challenges when investigating three-dimensional spatial domains with realistic geometries.

## Acknowledgements

The authors wish to thank Dr. A. Bressan and Prof. S. Scacchi for helpful preliminary discussions.

P. Tesini is supported by European Union - Next Generation EU via the PRIN project “ASTICE”.

L. Dedè acknowledges the support of the PRIN project 202232A8AN “Computational modeling of the human heart: from efficient numerical solvers to cardiac digital twins”, MUR, Italy.

G. Loli and G. Sangalli acknowledge support from PNRR-M4C2-I1.4-NC-HPC-Spoke6 and the PRIN 2022 PNRR project NOTES (No. P2022NC97R).

The authors are members of the Gruppo Nazionale Calcolo Scientifico - Istituto Nazionale di Alta Matematica (GNCS-INdAM).

M. Montardini acknowledges support from the PRINN 2022 PNRR project HEXAGON (No. P20227CTY3).

G. Loli, M. Montardini and P. Tesini are partially supported by INdAM-GNCS Project “Sviluppo di metodi numerici innovativi ed efficienti per la risoluzione di PDE”.



## References

- [1] T. J. R. Hughes, J. A. Cottrell, Y. Bazilevs, Isogeometric analysis: CAD, finite elements, NURBS, exact geometry and mesh refinement, *Computer Methods in Applied Mechanics and Engineering* 194 (39) (2005) 4135–4195. doi:10.1016/j.cma.2004.10.008.
- [2] J. A. Evans, Y. Bazilevs, I. Babuška, T. J. R. Hughes,  $n$ -widths, sup-infs, and optimality ratios for the  $k$ -version of the isogeometric finite element method, *Computer Methods in Applied Mechanics and Engineering* 198 (2009) 1726–1741. doi:10.1016/j.cma.2009.01.021.
- [3] A. Bressan, E. Sande, Approximation in FEM, DG and IGA: a theoretical comparison, *Numerische Mathematik* 143 (4) (2019) 923–942. doi:10.1007/s00211-019-01063-5.
- [4] K. Takizawa, T. Tezduyar, Space-time computation techniques with continuous representation in time (ST-C), *Computational Mechanics* 53 (1) (2014) 91–99. doi:10.1007/s00466-013-0895-y.
- [5] U. Langer, S. E. Moore, M. Neumüller, Space-time isogeometric analysis of parabolic evolution problems, *Computer Methods in Applied Mechanics and Engineering* 306 (2016) 342 – 363. doi:10.1016/j.cma.2016.03.042.



- [6] M. Montardini, M. Negri, G. Sangalli, M. Tani, Space-time least-squares isogeometric method and efficient solver for parabolic problems, *Mathematics of Computation* 89 (323) (2020) 1193–1227. doi:10.1090/mcom/3471.
- [7] G. Loli, M. Montardini, G. Sangalli, M. Tani, An efficient solver for space-time isogeometric Galerkin methods for parabolic problems, *Computers and Mathematics with Applications* 80 (11) (2020) 2586–2603. doi:10.1016/j.camwa.2020.09.014.
- [8] C. Saadé, S. Lejeunes, D. Eyheramendy, R. Saad, Space-Time Isogeometric Analysis for linear and non-linear elastodynamics, *Computers & Structures* 254 (2021) 106594. doi:10.1016/j.compstruc.2021.106594.
- [9] G. Loli, G. Sangalli, P. Tesini, High-order spline upwind for space-time Isogeometric Analysis, *Computer Methods in Applied Mechanics and Engineering* 417 (11) (2023) 116408. doi:10.1016/j.cma.2023.116408.
- [10] A. N. Brooks, T. J. R. Hughes, Streamline upwind/Petrov-Galerkin formulations for convection dominated flows with particular emphasis on the incompressible Navier-Stokes equations, *Computer Methods in Applied Mechanics and Engineering* 32 (1) (1982) 199–259. doi:10.1016/0045-7825(82)90071-8.
- [11] P. Colli Franzone, L. F. Pavarino, S. Scacchi, *Mathematical cardiac electrophysiology*, Vol. 13, Springer, 2014. doi:10.1007/978-3-319-04801-7.
- [12] A. Quarteroni, L. Dedè, A. Manzoni, C. Vergara, *Mathematical Modelling of the Human Cardiovascular System: Data, Numerical Approximation, Clinical Applications*, Cambridge Monographs on Applied and Computational Mathematics, Cambridge University Press, 2019. doi:10.1017/9781108616096.
- [13] P. Colli Franzone, L. F. Pavarino, S. Scacchi, *Mathematical and numerical methods for reaction-diffusion models in electrocardiology*, Springer Milan, Milano, 2012, pp. 107–141. doi:10.1007/978-88-470-1935-5\_5.
- [14] S. Krishnamoorthi, M. Sarkar, W. S. Klug, Numerical quadrature and operator splitting in finite element methods for cardiac electrophysiology, *International Journal for Numerical Methods in Biomedical Engineering* 29 (11) (2013) 1243–1266. doi:10.1002/cnm.2573.
- [15] M. Bendahmane, R. Bürger, R. Ruiz-Baier, A multiresolution space-time adaptive scheme for the bidomain model in electrocardiology, *Numerical Methods for Partial Differential Equations* 26 (6) (2010) 1377–1404. doi:10.1002/num.20495.
- [16] P. Colli Franzone, P. Deuffhard, B. Erdmann, J. Lang, L. F. Pavarino, Adaptivity in Space and Time for Reaction-Diffusion Systems in Electrocardiology, *SIAM Journal on Scientific Computing* 28 (3) (2006) 942–962. doi:10.1137/050634785.
- [17] J. Southern, G. Gorman, M. Piggott, P. Farrell, Parallel anisotropic mesh adaptivity with dynamic load balancing for cardiac electrophysiology, *Journal of Computational Science* 3 (1) (2012) 8–16. doi:10.1016/j.jocs.2011.11.002.
- [18] C. D. Cantwell, S. Yakovlev, R. M. Kirby, N. S. Peters, S. J. Sherwin, High-order spectral/hp element discretisation for reaction-diffusion problems on surfaces: Application to cardiac electrophysiology, *Journal of Computational Physics* 257 (2014) 813–829. doi:10.1016/j.jcp.2013.10.019.
- [19] A. S. Patelli, L. Dedè, T. Lassila, A. Bartezzaghi, A. Quarteroni, Isogeometric approximation of cardiac electrophysiology models on surfaces: An accuracy study with application to the human left atrium, *Computer Methods in Applied Mechanics and Engineering* 317 (2017) 248–273. doi:10.1016/j.cma.2016.12.022.
- [20] L. Pegolotti, L. Dedè, A. Quarteroni, Isogeometric Analysis of the electrophysiology in the human heart: Numerical simulation of the bidomain equations on the atria, *Computer Methods in Applied Mechanics and Engineering* 343 (2019) 52–73. doi:10.1016/j.cma.2018.08.032.

- [21] J. Rogers, A. McCulloch, A collocation-Galerkin finite element model of cardiac action potential propagation, *IEEE Transactions on Biomedical Engineering* 41 (8) (1994) 743–757. doi:10.1109/10.310090.
- [22] M. Courtemanche, R. J. Ramirez, S. Nattel, Ionic mechanisms underlying human atrial action potential properties: insights from a mathematical model, *American Journal of Physiology-Heart and Circulatory Physiology* 275 (1) (1998) H301–H321. doi:10.1152/ajpheart.1998.275.1.H301.
- [23] G. Loli, G. Sangalli, M. Tani, Easy and efficient preconditioning of the isogeometric mass matrix, *Computers & Mathematics with Applications* 116 (2022) 245–264, new trends in Computational Methods for PDEs. doi:10.1016/j.camwa.2020.12.009.
- [24] L. Beirão da Veiga, A. Buffa, G. Sangalli, R. Vázquez, Mathematical analysis of variational isogeometric methods, *Acta Numerica* 23 (2014) 157–287. doi:10.1017/S096249291400004X.
- [25] J. A. Cottrell, T. J. R. Hughes, Y. Bazilevs, *Isogeometric analysis: toward integration of CAD and FEA*, John Wiley & Sons, 2009.
- [26] Y. Wenjian, G. Yu, L. Yaohang, Efficient Randomized Algorithms for the Fixed-Precision Low-Rank Matrix Approximation, *SIAM Journal on Matrix Analysis and Applications* 39 (3) (2018) 1339–1359. doi:10.1137/17M1141977.
- [27] R. Vázquez, A new design for the implementation of isogeometric analysis in Octave and Matlab: GeoPDEs 3.0, *Computers & Mathematics with Applications* 72 (3) (2016) 523–554. doi:10.1016/j.camwa.2016.05.010.
- [28] L. Sorber, M. Van Barel, L. De Lathauwer, *Tensorlab v2.0*, Available online, January (2014). URL <http://www.tensorlab.net/>